TOWARDS ROBUST BEDSIDE HYPERSPECTRAL IMAGING: ACQUISITION-INDUCED SPECTRAL DISTORTIONS IN SKIN MEASUREMENTS

Thomas De Kerf [1], *Mathias Vanhoof*[1], *Jeroen Elegeert*[1] *Warre Clarys*[1], *Filip Thiessen*[2], *Steve Vanlanduit*[1], *Gunther Steenackers*[1]

[1]InViLab Research Group, University of Antwerp, Groenenborgerlaan 179, 2020 Antwerp, Belgium

[2]Department of Plastic, Reconstructive and Aesthetic Surgery, Multidisciplinary Breast Clinic, Antwerp University Hospital (UZA), University of Antwerp, Drie Eikenstraat 655, 2650 Edegem, Belgium

ABSTRACT

Skin hyperspectral imaging (HSI) enables non-invasive assessment of peripheral perfusion, with potential applications in sepsis monitoring, wound assessment and postoperative flap monitoring. For patients with limited mobility, bedside use requires positioning the camera on a bed-mounted or adjacent support to repeatedly image the same anatomical region. Patient movement, bed adjustments and changing illumination can compromise comparability between acquisitions. However, the finite acquisition time of HSI makes measurements susceptible to patient motion and changes in illumination, which may confound physiological interpretation and subsequent spectral classification. In this study, we investigate these failure modes through controlled experiments under conditions representative of bedside acquisition. We show that acquisition disturbances can shift measured hand reflectance spectra toward a reference associated with experimentally restricted blood flow, even when no flow-restriction intervention is applied during the disturbed acquisition. These findings highlight the need to distinguish acquisition-induced spectral variation from perfusion-related changes before HSI can reliably support bedside monitoring.

Index Terms— Hyperspectral imaging, skin, acquisition sensitivity, normalization, peripheral perfusion, sepsis

1 Introduction

Hyperspectral imaging (HSI) records spatially resolved skin spectra without contact. Clinical studies have reported a microcirculatory sepsis pattern and investigated spectral discrimination of critically ill patients [1, 2, 3]. These findings motivate bedside monitoring, where repeated measurements must remain comparable despite changes in positioning and illumination. Exposure, illumination, focus and geometry can affect spectral magnitude and shape, potentially confounding the interpretation of longitudinal changes. Normalization may suppress acquisition effects while also removing physiological information; spectral overlap after preprocessing therefore does not establish physiological robustness.

Previous studies evaluated optical parameters on reference targets [4], compared normalization methods [5], tested occlusion-sensitive indices under varying illumination [6], and investigated illumination calibration [7]. Building on this work, we examine controlled disturbances during spatial-scanning VNIR measurements of curved fingertip tissue. Repositioning can change illumination and viewing geometry, while transient movement or shadowing during acquisition can introduce distortions that depend on disturbance timing. Their effects must therefore be evaluated beyond changes in average signal magnitude.

This exploratory single-participant study examines how physical acquisition disturbances affect measured skin spectra under different preprocessing strategies. We quantify both displacement toward an experimentally acquired restricted-flow reference and distortion perpendicular to that direction. This distinguishes spectral changes resembling the reference contrast from other acquisition-related distortions. The study identifies failure modes relevant to repeated bedside measurements; it does not establish diagnostic accuracy or generalizability across participants.

2 Materials and Methods

2.1 Imaging setup and measurement protocol

Skin reflectance measurements were acquired using an Imec Snapscan VNIR hyperspectral camera covering 470-900 nm with 150 spectral bands. The camera was equipped with a 25mm lens and positioned at 25cm from the hand. Illumination was provided by a DC halogen lamp. Exposure time, gain and scan settings were held constant across conditions, giving a cube acquisition time of $T = [36.4]$ s.

This exploratory study involved one participant. The hand was supported using a 3D-printed mount attached to a zaber rotational stage. Measurements were acquired under undisturbed conditions and after controlled changes in hand orientation, focus and illumination. Each of the 34 acquisition conditions was measured in triplicate.

Undisturbed measurements were acquired first to provide matched baselines for the disturbed acquisitions. A restricted-flow reference was obtained using a cuff and 3 minutes of inflation. This reference represented the spectral change associated with the experimental restricted-flow condition.

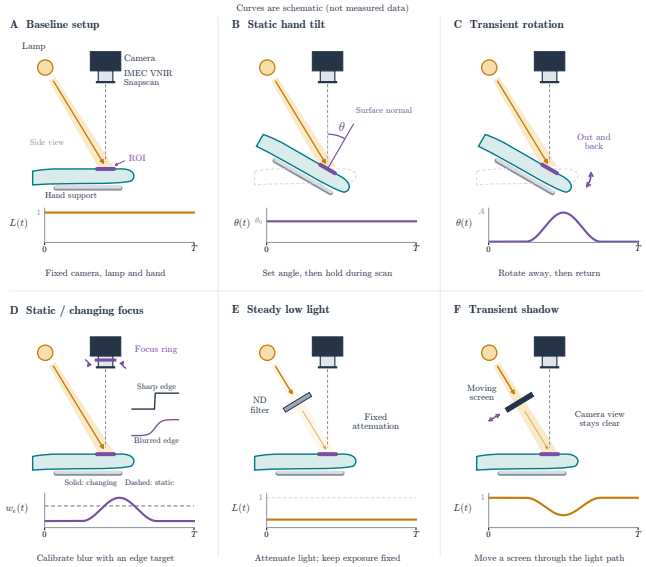


Fig. 1. Schematic overview of the physical acquisition conditions used for hand hyperspectral imaging. (A) Reference arrangement with a stationary camera, lamp, supported hand and reference patch. The purple surface segment marks the anatomical region of interest (ROI). (B) A fixed hand rotation changes the surface orientation and is maintained throughout the cube. The angle θ is measured relative to the baseline surface normal; positive rotation is away from the lamp. (C) Transient rotation moves the hand away from, and back toward, its baseline orientation during acquisition. (D) Defocus is introduced by adjusting the lens focus while keeping the hand position fixed. Focus settings are calibrated using a measured edge-spread width, w_e; the dashed and solid traces illustrate static and time-varying defocus, respectively. (E) A neutral-density (ND) attenuator reduces incident light throughout the cube. (F) A moving screen temporarily attenuates illumination without obstructing the camera view. Miniature plots illustrate the controlled quantity over one measured cube duration T: relative illumination $L(t)$, angle $\theta(t)$ or edge-spread width $w_e(t)$. The miniature traces schematically illustrate the disturbance profiles and do not represent recorded waveforms. Exposure, gain and acquisition settings were held constant across comparable conditions.

2.2 Acquisition disturbances

A schematic overview of the different experiments can be found in Figure 1.

Static tilt was evaluated at 15°, 30° and 45° relative to the baseline orientation, with positive rotation defined as movement away from the lamp. The hand remained stationary during each static acquisition. **Transient rotation** involved briefly tilting the hand away from its initial position and then returning it while the camera was recording. The maximum tilt was 30°. The hand reached its maximum tilt one-quarter, halfway or three-quarters through the acquisition ($T/4$, $T/2$ or $3T/4$, where T is the total acquisition time), to assess whether the timing of movement affected the measured spectra.

Static and changing defocus will be introduced by adjusting the lens focus while keeping the hand position, aperture, exposure and image resolution fixed. Focus settings will be calibrated using the 10–90% edge-spread width of a sharp edge target at the hand plane, measured at 550 nm. For a baseline width of approximately 30 pixels, static conditions will use widths of 60 and 120 pixels; changing-focus conditions will follow a $30 \rightarrow 120 \rightarrow 30$ pixel excursion lasting $T/2$, with peaks at $T/4$, $T/2$ or $3T/4$.

Steady low-light conditions will be produced by dimming the halogen lamp to target 50%, 10%, 1% and 0.1% of baseline illumination while keeping exposure fixed. **Transient shadowing** will temporarily reduce illumination to approximately 50% of baseline without obstructing the camera view. Each shadow excursion will last $T/2$, with its maximum attenuation centered at $T/4$, $T/2$ or $3T/4$.

2.3 Calibration and spectral preprocessing

Reflectance was calibrated using white-reference measurements. Focus was checked manually using a checkerboard target. Anatomical regions of interest were selected manually, and spectra were obtained by averaging the reflectance values over the selected ROI pixels. Five preprocessing configurations were compared: calibrated spectra without additional normalization, mean, maximum, min–max and standard-normal-variate (SNV) normalization.

Three calibrated ROI spectra were averaged before normalization. The resulting spectrum x_b was retained unchanged or transformed as follows:

$$\text{Mean:} \quad x_b/\mu_x, \tag{1}$$

$$\text{Maximum:} \quad x_b/\max_k x_k, \tag{2}$$

$$\text{Min–max:} \quad \frac{x_b - \min_k x_k}{\max_k x_k - \min_k x_k}, \tag{3}$$

$$\text{SNV:} \quad (x_b - \mu_x)/\sigma_x, \tag{4}$$

where $\mu_x = B^{-1}\sum_b x_b$ and $\sigma_x = [B^{-1}\sum_b (x_b - \mu_x)^2]^{1/2}$, with $B = 63$. Statistics were calculated across wavelengths for each triplicate-averaged spectrum.

2.4 Spectral evaluation

For each experiment and preprocessing method f, let $\mathbf{m}_f$ and $\mathbf{n}_f$ denote the mean preprocessed disturbed spectrum and matched normal baseline, respectively, and let $\mathbf{r}_f$ denote the corresponding preprocessed restricted-flow reference. Means were calculated over 3 separate measurements. With $\mathbf{d}_f = \mathbf{r}_f - \mathbf{n}_f$, projected spectral movement was quantified as

$$S_f = 100\,\frac{(\mathbf{m}_f - \mathbf{n}_f)^\top \mathbf{d}_f}{\|\mathbf{d}_f\|_2^2}. \tag{5}$$

All wavelength bands were weighted equally. A value of 0% indicates no projected movement, 50% indicates the midpoint along the normal–restricted direction, and 100% indicates the restricted endpoint's projected position. Negative values indicate movement in the opposite direction, while values above 100% indicate overshoot. This measure describes directional spectral displacement; it does not imply an exact spectral match, a classification probability or a percentage change in blood flow.

3 Results

Twelve acquisition conditions and five preprocessing configurations are shown to illustrate the key findings; results for all evaluated conditions and preprocessing configurations are provided in the Supplementary Information. Figure 3 shows the projected movement of

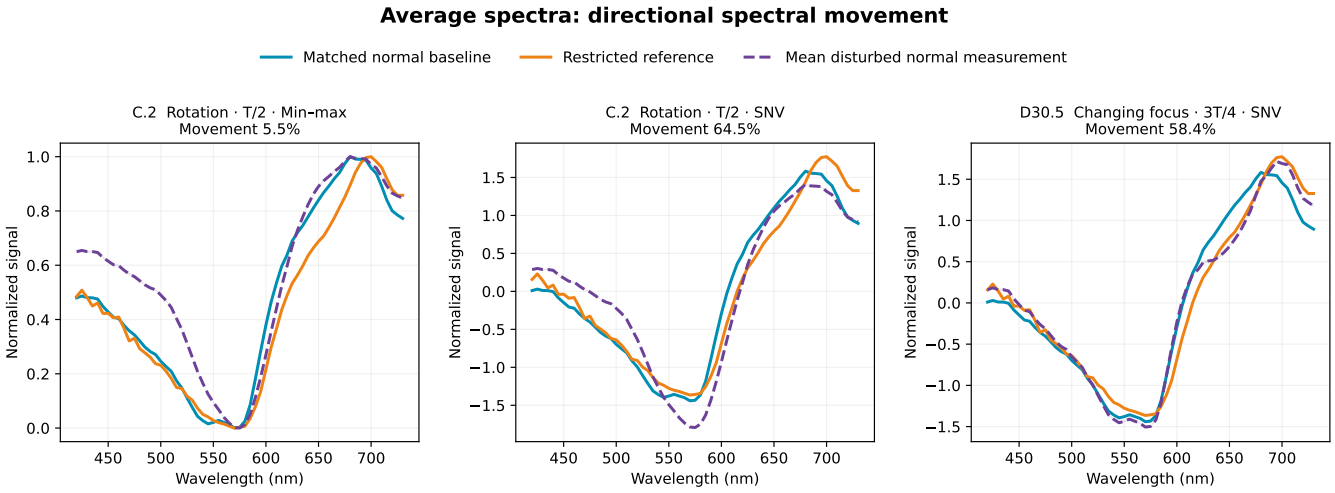


Fig. 2. Mean measured spectr'a for selected acquisition disturbances and normalization methods. Curves show the matched normal baseline, restricted-flow reference and disturbed acquisition obtained without an intended flow-restriction intervention. Annotations report projected displacement toward restricted flow and perpendicular (off-axis) distortion, both expressed relative to the normal–restricted spectral separation. The focus example corresponds to the stronger changing-focus condition peaking at $3T/4$.

the average simulated measurement relative to the normal–restricted spectral separation. Here, 0% indicates no displacement along this direction, whereas 100% corresponds to the projected position of the restricted reference. Values above 100% indicate overshoot and do not imply greater similarity to restricted flow.

Static disturbances were largely compensated by normalization. Without additional normalization, a 30° tilt (B.2), static defocus from 30 to 120 pixels (D30.2), and illumination reduced to 50% of baseline (E.1) produced shifts of 196.4%, 49.2%, and 232.4%, respectively. Mean, maximum, min–max and SNV normalization reduced these projected shifts to approximately zero under the tested conditions.

Transient disturbances showed a strong dependence on timing and preprocessing. For rotation peaking at $T/2$ (C.2), where T denotes the scan duration, SNV and min–max normalization yielded shifts of 64.5% and 5.5%, respectively. Moving the disturbance to $3T/4$ (C.3) increased these values to 312.0% and 308.3%. Earlier rotation at $T/4$ (C.1) instead produced negative shifts with both methods. A similar timing dependence occurred for transient shadowing: SNV yielded 79.0% at $T/2$ (F.2) and 364.6% at $3T/4$ (F.3). Changing focus also produced greater displacement with SNV for the late excursion (D30.5; 58.4%) than for the early excursion (D30.3; −6.6%). Thus, normalization that suppressed static disturbances did not consistently suppress disturbances occurring during sequential acquisition.

Reduced illumination further differentiated the methods. At 1% illumination (E.3), maximum normalization retained a shift of 23.0%, compared with 0.1% for mean normalization and 0.7% for SNV. At 0.1% illumination (E.4), these values were 265.6%, 1.1%, and 19.9%, respectively. However, E.4 was flagged as low SNR.

Overall, the results show that the effectiveness of normalization depends on disturbance type, timing and illumination level.

3.1 Interpretation of projected spectral movement

The overlays in Fig. 2 illustrate that a small projected shift does not necessarily imply preservation of spectral shape. For rotation peaking at $T/2$ (C.2), min–max normalization yielded a shift of only 5.5%, although the average disturbed spectrum visibly differed from the normal baseline, particularly at shorter wavelengths. With SNV, the same disturbance produced a shift of 64.5%, while the disturbed spectrum still differed from the restricted reference. Thus, projected movement summarizes displacement along the normal–restricted direction without establishing a complete spectral match.

Focus results also depended on whether defocus remained constant or changed during acquisition. Static defocus from 30 to 120 pixels (D30.2) produced approximately zero projected displacement after normalization. For the changing-focus excursion peaking at $3T/4$ (D30.5), however, min–max and SNV yielded shifts of 52.3% and 58.4%, respectively. The SNV overlay shows partial convergence toward the restricted reference, with differences remaining across the spectrum.

3.2 Transient shadowing and low illumination

Transient shadowing produced substantial residual displacement after normalization. For a shadow peaking at $T/2$ (F.2), projected shifts were 15.1% with min–max normalization and 79.0% with SNV. At $3T/4$ (F.3), these increased to 304.3% and 364.6%, respectively. This timing dependence reinforces that normalization does not consistently compensate for illumination changes during sequential acquisition.

Under steady illumination reduced to 1% of baseline (E.3), projected shifts were 23.0% with maximum, 6.0% with min–max and 0.7% with SNV normalization. At 0.1% illumination (E.4), the corresponding values increased to 265.6%, 39.9% and 19.9%. This condition was flagged as low SNR and is presented as a diagnostic average. A small displacement of an averaged spectrum therefore

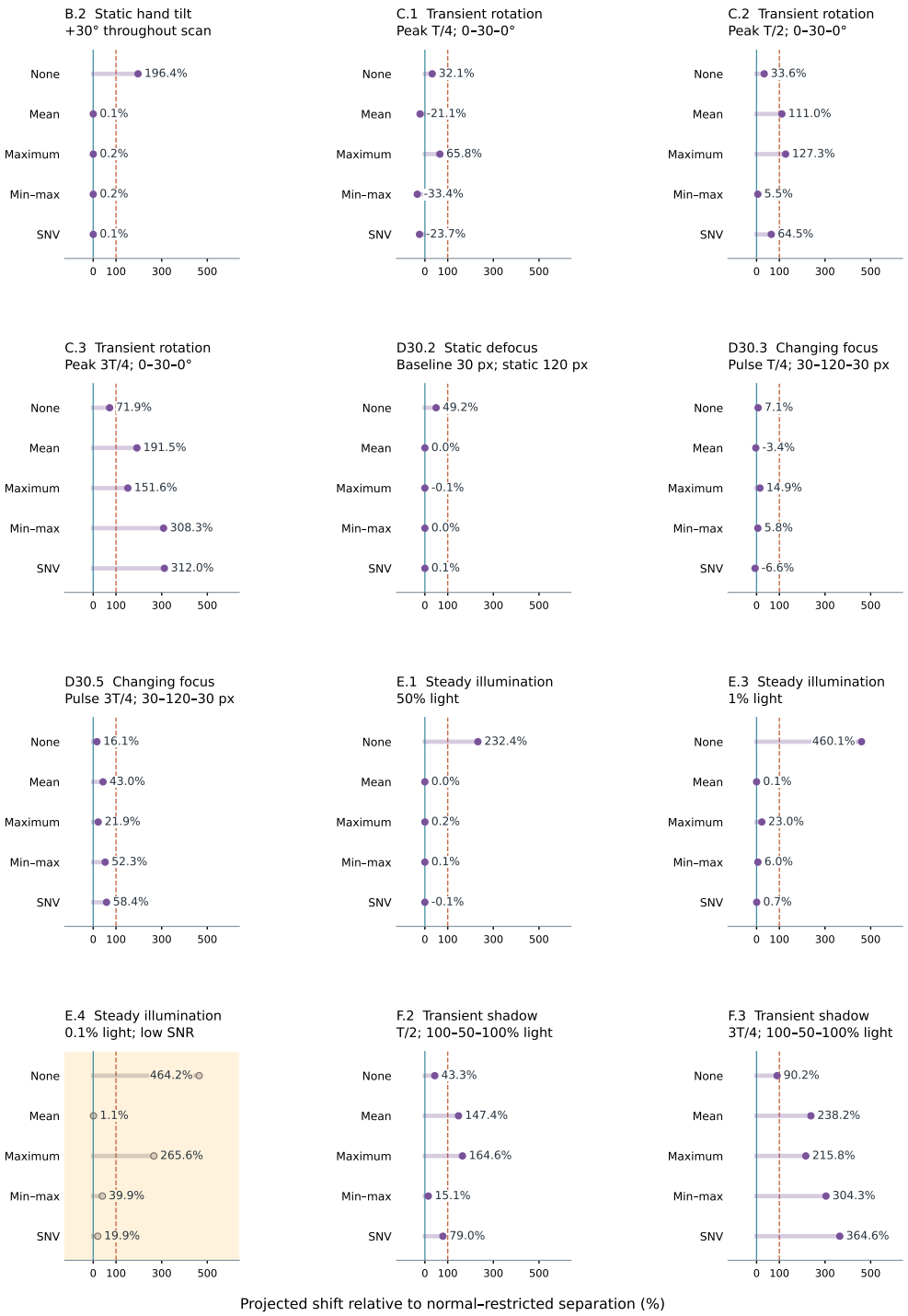


Fig. 3. Projected displacement of the average measured normal-state hand spectrum toward the restricted-flow reference for selected acquisition conditions and preprocessing methods. Values are expressed relative to the normal–restricted spectral separation: 0% denotes no projected displacement, 100% denotes the projected position of the restricted-flow reference, and values above 100% indicate overshoot. A displacement of 100% does not imply an exact spectral match because perpendicular distortion may remain. Conditions D30.2, D30.3 and D30.5 represent the stronger-defocus measurements.

should not be interpreted as evidence of reliable individual measurements.

4 Conclusion

5 Discussion and Conclusions

Acquisition disturbances shifted normal-hand spectra toward, and sometimes beyond, the projected position of a restricted-flow reference despite unchanged perfusion. Normalization substantially reduced projected displacement under static tilt, defocus and moderate dimming, but its effectiveness depended on disturbance type and timing. No evaluated method consistently maintained near-zero displacement across all conditions.

These findings suggest that preprocessing robustness should be assessed against both stable and transient acquisition disturbances. A method that compensates for a constant intensity change may remain inadequate when different parts of a reconstructed spectrum are affected unequally during acquisition. Consequently, performance under static conditions alone does not establish suitability for repeated bedside monitoring.

For bedside applications, these results motivate combining normalization with acquisition-quality assessment, including checks for motion, reference-patch stability and signal adequacy. Such checks should identify unreliable acquisitions while preserving sensitivity to physiological changes. The present simulation results identify potential failure modes; experimental validation across repeated measurements and multiple participants is required to establish their magnitude and clinical relevance.

6 Future Work

Future work should extend this single-participant study to a larger cohort spanning different skin pigmentation, including clinical populations. Repeated measurements under normal and restricted-flow conditions are needed to assess between-participant variability and evaluate classification performance on independent participants.

Experiments should also combine disturbances, vary their timing relative to wavelength acquisition, and compare acquisition orders where supported. Reference placement and multiple reference regions should be evaluated under spatially uneven illumination.

Finally, automated quality control should identify unreliable measurements and prompt immediate reacquisition. Normalization and rejection strategies should be assessed jointly using spectral fidelity, SAM or cosine-based classification, and rejection rates, rather than the visual overlap of average spectra alone.

7 Acknowledgements

This research was funded by the Research Foundation Flanders (FWO) under a Strategic Basic Research (SB) fellowship [1SB9825N] (Clarys Warre), by the FWO under a grant for Applied Biomedical Research with a Primary Social Goal [T001723N] and under an FWO postdoctoral scholarship [12A6126N] (De Kerf Thomas). The study was approved by the local ethics committee under Belgian registration number B3002024000116, and all participants provided written informed consent.

8 References

[1] Maximilian Dietrich, S. Marx, Maik von der Forst, et al., "Bedside hyperspectral imaging indicates a microcirculatory sepsis pattern—an observational study," *Microvascular Research*, vol. 136, pp. 104164, 2021.

[2] Judith Kohnke, Kevin Pattberg, Felix Nensa, et al., "A proof of concept for microcirculation monitoring using machine learning based hyperspectral imaging in critically ill patients: a monocentric observational study," *Critical Care*, vol. 28, no. 1, pp. 230, 2024.

[3] Silvia Seidlitz, Katharina Hölzl, Ayca von Garrel, et al., "AI-powered skin spectral imaging enables instant sepsis diagnosis and outcome prediction in critically ill patients," *Science Advances*, vol. 11, no. 29, pp. eadw1968, 2025.

[4] Siavash Mazdeyasna, Mohammed Shahriar Arefin, Andrew Fales, Silas J. Leavesley, T. Joshua Pfefer, and Quanzeng Wang, "Evaluating the performance of hyperspectral imaging endoscopes: Mitigating parameters affecting spectral accuracy," *Biosensors*, vol. 15, no. 11, pp. 738, 2025.

[5] Siavash Mazdeyasna, Mohammed Shahriar Arefin, Andrew Fales, et al., "Evaluating Normalization Methods for Robust Spectral Performance Assessments of Hyperspectral Imaging Cameras," *Biosensors*, vol. 15, no. 1, pp. 20, 2025.

[6] Jens De Winne, Anoek Strumane, Danilo Babin, Siri Luthman, Hiep Luong, and Wilfried Philips, "Multispectral indices for real-time and non-invasive tissue ischemia monitoring using snapshot cameras," *Biomedical Optics Express*, vol. 15, no. 2, pp. 641–655, 2024.

[7] Alexander Baumann, Leonardo Ayala, Alexander Studier-Fischer, Jan Sellner, Berkin Özdemir, Karl-Friedrich Kowalewski, Slobodan Ilic, Silvia Seidlitz, and Lena Maier-Hein, "Deep intra-operative illumination calibration of hyperspectral cameras," in *Medical Image Computing and Computer Assisted Intervention – MICCAI 2024*. 2024, pp. 120–131, Springer Nature Switzerland.